A Molecular Dynamics Study of Ca^{2+}-Calmodulin: Evidence of Interdomain Coupling and Structural Collapse on the Nanosecond Timescale

Craig M. Shepherd and Hans J. Vogel
Structural Biology Research Group, Department of Biological Sciences, University of Calgary, Calgary, Alberta T2N 1N4, Canada

ABSTRACT A 20-ns molecular dynamics simulation of Ca^{2+}-calmodulin (CaM) in explicit solvent is described. Within 5 ns, the extended crystal structure adopts a compact shape similar in dimension to complexes of CaM and target peptides but with a substantially different orientation between the N- and C-terminal domains. Significant interactions are observed between the terminal domains in this compact state, which are mediated through the same regions of CaM that bind to target peptides derived from protein kinases and most other target proteins. The process of compaction is driven by the loss of helical structure in two separate regions between residues 75–79 and 82–86, the latter being driven by unfavorable electrostatic interactions between acidic residues. In the first 5 ns of the simulation, a substantial number of contacts are observed between the first helix of the N-terminal domain and residues 74–77 of the central linker. These contacts are correlated with the closing of the second EF-hand, indicating a mechanism by which they can lower calcium affinity in the N-terminal domain.

INTRODUCTION

Members of the EF-hand family of proteins respond to cellular calcium influxes by selectively binding calcium ions in highly conserved helix-loop-helix motifs. Calcium-induced conformational changes in regulatory members of this family cause them to bind and regulate target enzymes involved in a wide variety of metabolic and mechanical processes. Calmodulin (CaM) is a highly conserved EF-hand protein of 148 residues found in all eukaryotic cells and is responsible for the regulation of well over 100 different target proteins (Hoeflich and Ikura, 2002; Yamniuk and Vogel, 2004). Under crystallization conditions, Ca^{2+}-CaM adopts a dumbbell structure in which the globular N- and C-terminal lobes are separated by a single α-helix of eight turns. This central linker helix is largely exposed to the solvent (Babu et al., 1988; Chattopadhyaya et al., 1992; Wilson and Brunger, 2000). The terminal lobes each consist of two helix-loop-helix domains (EF-hands) and are in roughly a *trans* orientation with respect to each other on either side of the central helical linker. Each of the EF-hands is capable of coordinating a single calcium ion. Calcium binding causes helical rearrangements in both of the terminal domains, exposing large hydrophobic clefts responsible for binding to target proteins (Chou et al., 2001; Yuan et al., 1999a,b).

Before the determination of high-resolution CaM structures, small angle x-ray scattering (SAXS) studies (Heidorn and Trewhella, 1988; Trewhella and Krueger, 2002) and NMR measurements (Barbato et al., 1992; Spera et al., 1991) indicated that the central helix linker is more flexible than implied from the crystal structure. Crystal (Meador et al., 1992) and NMR (Ikura et al., 1992) structures of Ca^{2+}-CaM bound to target peptides from CaM-dependent kinases reveal a large conformational change upon binding: a short region of α-helical structure in the middle of the central linker is broken (Ikura et al., 1992; Meador et al., 1992). This enables the terminal lobes to reorient and wrap around the target peptide, although different binding modes have also been found (Hoeflich and Ikura, 2002; Yamniuk and Vogel, 2004; Yap et al., 2003; Ishida and Vogel, 2004). Interactions between CaM and the target peptide are mediated almost exclusively by side-chain–side-chain interactions; the large hydrophobic clefts exposed by calcium binding are formed mainly from methionine and other hydrophobic residues. These hydrophobic residues are surrounded by negatively charged residues, forming ideal binding surfaces for the interaction with hydrophobic/positively charged amphipathic target peptides, which form ideal α-helices in the complexes. The induction of α-helical structure by Ca^{2+}-CaM is believed to be a critical step in the activation process of target proteins (Yuan et al., 1999b)

A topic of considerable interest is the interdomain coupling that occurs between the N- and C-terminal lobes of CaM: despite their large average separation, calcium binding between the high-affinity C-terminal lobe and the lower affinity N-terminal lobe is cooperative. Shea and co-workers have shown that basic residues between 74 and 77 in the central linker are critical to the communication between the N- and C-terminal domains (Faga et al., 2003). Using sequential single residue additions to a construct consisting of residues 1–74 of *Paramecium* CaM ($PCaM_{1-74}$), stepwise decreases in calcium binding affinity and stepwise increases in melting temperatures were observed by introducing residues up to and including Lys-77. The further addition of residues 78–80 had little observable effect (Faga et al., 2003).

Submitted August 19, 2003, and accepted for publication April 20, 2004.

Address reprint requests to Hans J. Vogel, Tel.: 403-220-6006; Fax: 403-289-9311; E-mail: vogel@ucalgary.ca.

0006-3495/04/08/780/12 $2.00

doi: 10.1529/biophysj.103.033266

CaM has been the subject of many computational studies. Early molecular dynamics (MD) simulations of Ca^{2+}-calmodulin supported the notion of flexibility in the central helix (Mehler et al., 1991; Vorherr et al., 1992; Weinstein and Mehler, 1994). Due to limited computational power available at the time, these simulations were carried out over sub-nanosecond timescales and included relatively few, if any, water molecules. Van der Spoel et al. (1996) performed a 3-ns simulation of the CaM central helix (residues 65–92) in explicit solvent. The results indicated that the flexibility of the linker region was an inherent property of the central helix. Simulations of a similar length have now been reported for Ca^{2+}-CaM (Komeiji et al., 2002; Van der Spoel et al., 1996; Wriggers et al., 1998; Yang et al., 2001) and apo-CaM (Yang and Kuczera, 2002). These latter simulations all employ bulk solvation with explicit water molecules and counterions. In a recent 3-ns simulation of the calcium loaded N-domain of CaM, Vigil et al. (2001) observed a transition from an open to a closed state, in which the solvent-exposed hydrophobic cleft becomes buried. This showed that the transition from an open to a closed state, which is caused by a reorientation of the helices within EF-hand domains (Yap et al., 2002), can occur on the nanosecond timescale and that closed orientations can occur even when calcium ions are bound at both sites.

In addition to simulations of CaM, the structures of a large number of EF-hand proteins have been solved by either x-ray crystallography or NMR. This has allowed a structural analysis of the conformational changes occurring in EF-hand domains in response to the binding of calcium (Yap et al., 2002). Vector geometry mapping (VGM) analysis (see Materials and Methods) of CaM in the calcium-loaded and calcium-free states shows a distinct change in the orientation of the EF-hand helices, defining an ''open'' and a ''closed'' state, respectively (Yap et al., 1999). Upon binding calcium, there is an increase in the interhelical angle (θ), a decrease in ϕ (a clockwise swing of the exiting helix about the entering helix), and a large decrease in ω (a large clockwise twist motion about the exiting helix axis).

Taken together, the results of past simulation studies and structural analyses of CaM have provided a detailed, dynamic view of this protein that is consistent with experimental results. However, improvements in simulation methodology and computational power have made it possible to increase the timescales hitherto examined. Here we present the results of a 20-ns simulation of Ca^{2+}-CaM in solution, performed to examine the possibility of explicit interactions between the terminal lobes of CaM and between these domains and the central linker region.

MATERIALS AND METHODS

Molecular dynamics simulations

The simulation and all analyses other than vector geometry mapping (see below) were performed with the GROMACS software package, version 3.0 (Lindahl et al., 2001). The starting structure for the simulation of Ca^{2+}-CaM was taken from PDB entry 3CLN (Babu et al., 1988). Since the first four residues and the C-terminal residue were not observed in the x-ray diffraction studies, these were added to the structure in an extended conformation using InsightII (Accelrys, San Diego, CA). The protein was then placed in a cubic box with an edge length of 80 Å and solvated with simple point charge (SPC) water molecules (Berendsen et al., 1981) as described elsewhere (Van der Spoel et al., 1996). Based on the electrostatic potential calculated at water oxygen positions, 15 water molecules were replaced by sodium counterions to render the system electrostatically neutral. The final system, consisting of 50,464 atoms, was energy minimized using a steepest descent algorithm. Further relaxation of the solvent was achieved by a 500-ps position restraint simulation at 300 K in which an isotropic force constant of 100 kJ mol^{-1} $Å^{-1}$ was applied to all nonhydrogen protein atoms. The final configuration from the position restraint simulation provided the starting coordinates for the 20-ns production run. The mass of hydrogen atoms was increased by a factor of two to allow a time step of 4 fs and increase the efficiency of the simulation (Feenstra et al., 1999). Constant temperature and pressure were maintained through weak coupling to an external bath (Berendsen et al., 1984) of 300 K and 1 bar using coupling constants of 0.1 and 0.5 ps, respectively. Electrostatic interactions were calculated using the PME algorithm with a real space cutoff of 9.0 Å, fourth order spline interpolation, and a Fourier grid spacing of 1.2 Å. Van der Waals interactions were truncated at 10 Å. The neighbor list was updated every three steps of the dynamics. Coordinates were recorded every picosecond. All interaction parameters were taken from the Gromos-87 force field (van Gunsteren and Berendsen, 1987) with some modifications (Jorgensen et al., 1983; Liu et al., 1995; Mark et al., 1994; van Buuren et al., 1993).

Vector geometry mapping

Vector geometry mapping is a straightforward method developed specifically for analyzing conformational changes in EF-hand domains but in principle can be used for changes in the relative orientations of any two helices (Yap et al., 1999, 2002). First, a coordinate system is defined using the two helices of a reference EF-hand domain. Changes in the relative orientation and separation of helices in query EF-hand domains are measured within the coordinate system of the reference. As in the study of Yap et al. (1999), we have used EF-hand I from the solution structure of apo-CaM (Zhang et al., 1995) as the reference conformation. The orientation of the helices in a query EF-hand relative to the reference is described by three angles θ, ϕ, and ω, where θ is the angle between the exiting helix of the test EF-hand with the z axis, ϕ is the angle between this helix and the x axis, and ω is the counterclockwise rotation of the helix about its long axis with respect to the exiting helix of the reference (Fig. 8 *A* for a schematic).

RESULTS

Conformational changes

Fig. 1 *A* shows the root mean-square deviation (RMSD) of the Cα atoms in the simulation with respect to CaM in the extended crystal structure (Babu et al., 1988) and in the CaM-smooth muscle myosin light chain kinase peptide (smMLCKp) complex (Meador et al., 1992; PDB ID: 1CLN), respectively. Within the first nanosecond, the RMSD with respect to the extended structure rapidly increases to a value near 9 Å. After fluctuating around this value for a further 3 ns, the RMSD increases again between 4 and 5 ns to a value of ~13 Å. After this point, the simulated conformations remain at a relatively constant distance from the

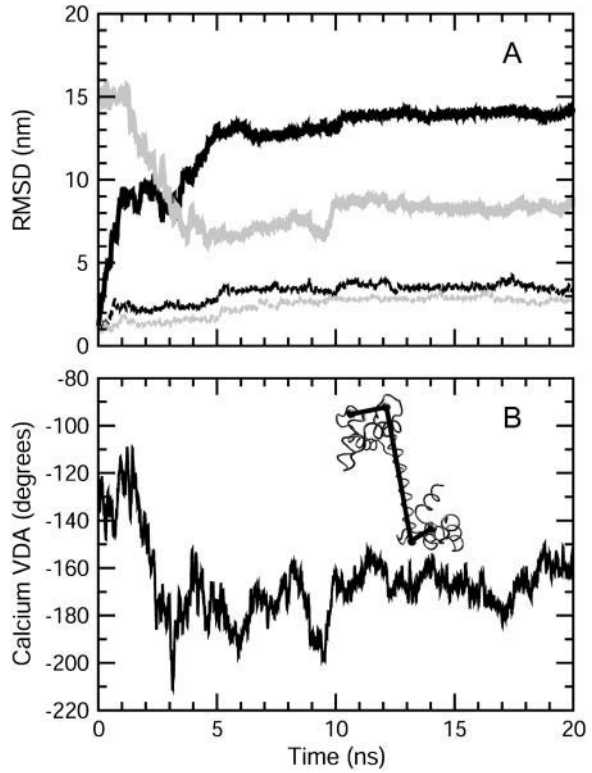

FIGURE 1 (*A*) Cα RMSD of calmodulin in the simulation. The thick solid and shaded lines show the RMSD with respect to the extended crystal structure (Babu et al., 1988) and calmodulin in the CaM-smMLCKp crystal structure (Meador et al., 1992), respectively. Thin solid and shaded lines show the RMSD of the N-terminal and C-terminal domains relative to the extended crystal structures using independent fits to residues 5–77 and 78–148, respectively. (*B*) Calcium virtual dihedral angle as a function of simulation time. (*Inset*) Schematic showing the definition of the VDA.

crystal structure. The drastic changes in the RMSD values relative to the crystal structure are clearly indicative of a large global conformational change. The newly adopted conformation is quite stable: pairwise comparison of structures from the last 10 ns of the simulation results in an average RMSD of 0.78 Å.

With respect to the CaM-smMLCKp complex, the RMSD remains relatively constant for approximately the first 2 ns and then decreases in a linear manner to a value of ~6.5 Å at the 5-ns mark. A small increase to a value of ~8 Å is seen at ~10 ns, and the RMSD fluctuates close to this value for the remainder of the simulation. The decrease in the value near the beginning of the simulation indicates that calmodulin adopts a much more compact state, as is the case in the binding of calmodulin to typical peptide targets. However, the large RMSD observed in the last 10 ns (8 Å) shows that although compact the conformations sampled during this time differ significantly from that of the CaM-smMLCKp complex.

Fig. 1 *A* also shows the Cα RMSD with respect to the extended crystal structure for the N-terminal and C-terminal domains alone, determined from independent fits using residues 5–77 and 78–148, respectively. The RMSD for the individual domains in the CaM simulation are much smaller in magnitude than those seen for the entire protein. This is consistent with a conformational change in which structure is maintained within each terminal domain and indicates that the large rise in RMSD is the result of changes within the central linker region. A pairwise comparison of structures from the last 10 ns of the simulation results in average RMSD values of 1.37 and 0.81 Å for the N- and C-terminal lobes, respectively. This is consistent with earlier simulations (Barton et al., 2002; Komeiji et al., 2002; Wriggers et al., 1998; Yang et al., 2001) of Ca^{2+}-CaM, which show the N-terminal to be more flexible than the C-terminal domain in the calcium-bound state. It should be noted that the opposite trend is observed in apo-CaM: an inverse relationship between thermostability and calcium affinity in the two terminal domains implies a higher flexibility for the C-terminal lobe in this case (Masino et al., 2000). It is likely that this increased flexibility allows the C-domain to more effectively accommodate the calcium ions during binding.

Previously, a virtual dihedral angle (VDA) defined by the four calcium ions has been used as a rough measure of the interdomain orientation in CaM. Changes in the relative orientation of the terminal domains cause the VDA to move from the value in the crystal structure (−134°) to values more consistent with a *cis* orientation for the two domains, as in a CaM-peptide complex (Wriggers et al., 1998). Fig. 1 *B* shows the calcium VDA from the simulation. Within the first nanosecond, the VDA decreases slightly and then increases to the value found in the CaM-smMLCKp complex (−110°) at ~1.5 ns. After this, however, the VDA decreases again and oscillates around values of ~−180° for the next 7 ns, reaching a minimum of about −220° at around the 3-ns mark. After a sharp dip to a value of about −200° at ~9 ns, the angle then increases and stabilizes to a value of −170° at around 10 ns. Thus, the VDA near the end of the simulation is more similar to the value found in the crystal structure, rather than that of the CaM-peptide complex. This explains the large RMSD between the simulated conformations and calmodulin in the CaM-smMLCKp complex.

Fig. 2 shows snapshots of calmodulin from the simulation. Visual inspection of the structures shows that with the exception of the central helix, all elements of secondary structure are essentially stable over the course of the simulations. A more detailed analysis using the DSSP program (Kabsch and Sander, 1983) revealed some minor unwinding of the helix A near the N-terminus and some transient breaking of hydrogen bonds in the β-sheets connecting individual EF-hand domains in both terminal lobes (data not shown). All calcium ions remain tightly coordinated throughout the simulation.

Structures from the plateau region of the RMSD between 1 and 4 ns are characterized by a disruption of the central linker helix, resulting in a conformation that is bent relative to the extended starting structure. Snapshots from 5 and 10 ns show

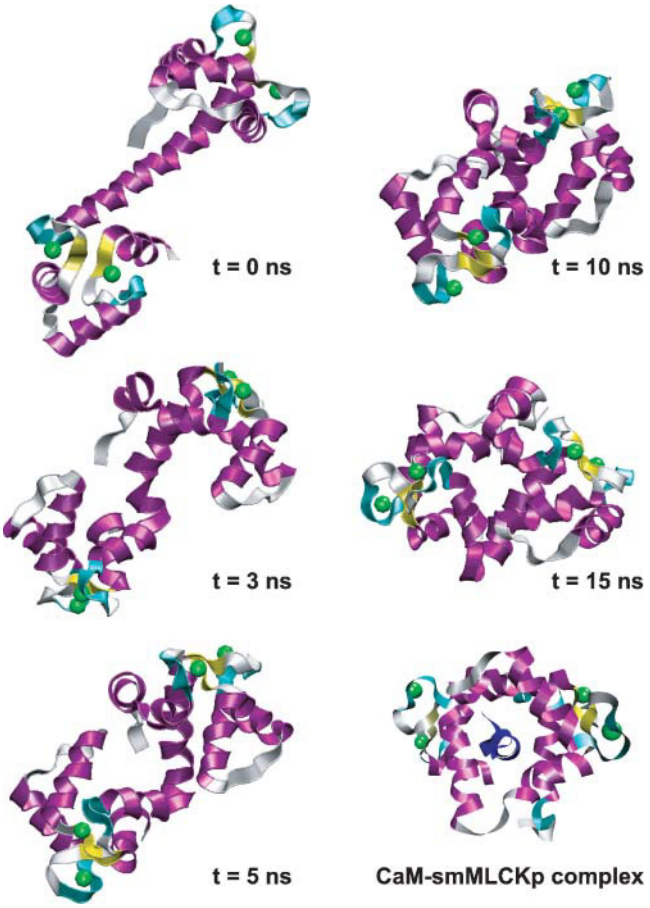

FIGURE 2 Structures from the simulation. α-Helices are shown in magenta, turns in blue, β-sheet in yellow, and coil in white. Calcium ions are shown in green. The structure of the CaM-smMLCKp complex (Meador et al., 1992) is shown for comparison, with the smMLCKp shown in dark blue. The figure was made with the program VMD (Humphrey et al., 1996).

a progressively greater compaction of the structure, in correlation with the subsequent increases in the RMSD. Shortly after the 5-ns mark of the simulation, the N- and C-terminal lobes interact directly with each other. After this point, the solvent accessible surface area (SASA) of CaM is slightly <95% of the value in the crystal structure. Many of the interactions formed between the domains result from side-chain–side-chain distances <5 Å (see Figs. 6 and 9). The structure does not change significantly in the last 10 ns of the simulation; the structure from 15 ns is included to provide an alternate perspective. The crystal structure of the CaM-smMLCKp complex (Meador et al., 1992), shown for comparison, has similar overall dimensions to the simulated compact state. At first glance, the conformation of calmodulin in both structures may seem deceptively similar: the snapshot from 15 ns even appears to contain a channel capable of accommodating an α-helical target peptide. However, as a result of the *trans* orientation of the domains in the compact state of the simulation, this structure is significantly different from that of CaM in the CaM-smMLCKp complex (see Fig. 1). Due to the difference in the orientation of the terminal domains, the channel in the simulated conformation is not lined by the same residues responsible for the binding of target peptides.

Helix breaking and side-chain–side-chain interactions

Fig. 3 *A* shows the secondary structure of the central linker region as a function of simulation time, whereas Fig. 3 *B* shows the same data as an average over the whole simulation. Two distinct regions of the central linker region lose helical structure in the simulation: in the first, residues 75–79 undergo moderate unfolding to bend, turn, and 3_{10}-helical conformations. The stability of this α-helical turn is substantial, with a minimum of 40% helical content at residue 78 (see Fig. 3 *B*). The disorder in this region at times spreads to residues 80 and 81, which fluctuate between α-helical and other conformations during the simulation (Fig. 3 *A*) but

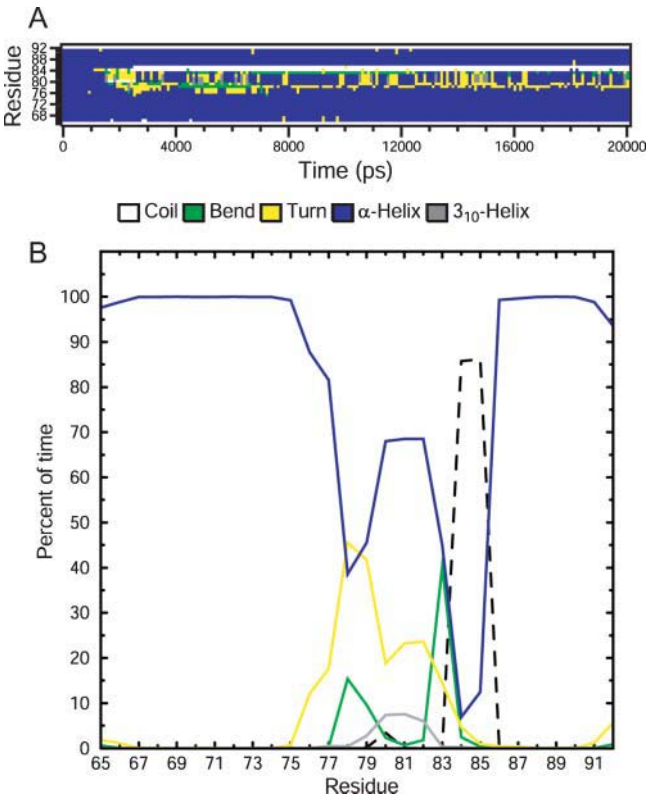

FIGURE 3 Secondary structure of the central linker region (residues 65–92) during the simulation. (*A*) Secondary structure as a function of simulation time. Residue numbers and time are shown along the *x* and *y* axes, respectively. The secondary structure of each residue was calculated every 40 ps of the simulation using the DSSP program (Kabsch and Sander, 1983) and colored according to the legend. (*B*) Secondary structure of the central linker region as an average over the entire simulation. The percentage of total simulation time spent by each residue in each of the secondary structure types is shown. Secondary structure was calculated as in *A*. Colors are according to the legend, with the exception of coil, which is shown as a dashed line.

retain an average of ~70% α-helical content. The loss of helical structure between residues 75–81 of the central linker is in good agreement with ^{15}N order parameters (Barbato et al., 1992) and earlier simulations (Wriggers et al., 1998; Yang et al., 2001) of Ca^{2+}-CaM. The second break in the helix between residues 82–86 is much more drastic, with the loss of a whole helical turn to a random coil conformation. Fig. 3 *A* shows that this break is actually the first to occur in the simulation, with the loss of helical structure to bend and turn conformations just after 1 ns and a complete breakdown to coil structure at around 2.5 ns. These residues remain unstructured for the remainder of the simulation. We observe large fluctuations in the distances between acidic side-chain pairs in the region around the second helical break before and during the conformational change taking place in the simulation (data not shown). After the compaction process at around 5 ns, these distances stabilize to large values. Thus it would seem that electrostatic repulsions between these acidic residues contribute to the loss of this α-helical turn. In addition, the loss of a helix-stabilizing electrostatic interaction between the side chains of Glu-82 and Arg-86 appears to be a key feature in the breaking of the central helix in this region. The distance between these two side chains and the α-helical content of residues 65–92 is shown in Fig. 4. For approximately the first 750 ps, the distance between the two side chains remains well below 5 Å, which can be considered an upper distance for a salt bridge between the two residues (Aliste et al., 2003). As the compaction process continues, the distance between the two side chains increases. Shortly after the distance exceeds the 5 Å limit, the α-helical content of the linker region starts to decrease, with the formation of a turn at residue 84.

Another important side-chain–side-chain interaction involving Glu-82 is a hydrogen bond with the phenol moiety of Tyr-138. The distance between these two side chains is also shown in Fig. 4. For about the first 400 ps, the Glu-82–Tyr-138 distance is stable at around 2 Å, and the two side chains are hydrogen bonded to each other during this time. With the insertion of a water molecule into this hydrogen bond at around 400 ps, the distance between the two side chains jumps suddenly to ~3.5 Å but remains stable up until 500 ps. The complete loss of this solvent-mediated hydrogen bond results in a total loss of interaction between the two groups, and the distance increases to large values concomitant with the loss of helical structure and the overall compaction of the protein.

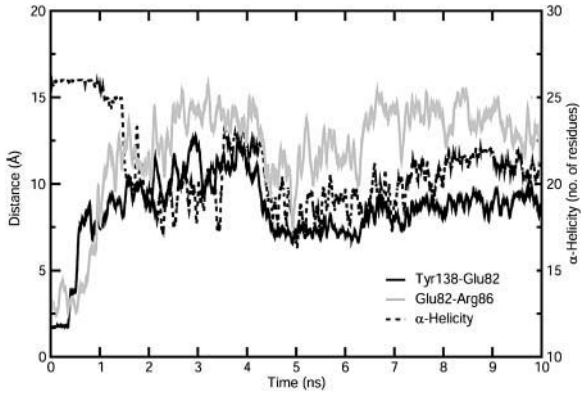

FIGURE 4 Role of selected side-chain–side-chain interactions in the compaction of CaM. The minimal distance between any two atoms of the relevant side chains is plotted as a function of simulation time. Also shown is the helicity of the central linker region (residues 65–92), based on the number of residues in an α-helical conformation. Distance and helicity scales are shown along the right and left axes, respectively. Lines are displayed according to the legend.

The compact state

A reduction in the overall dimensions of CaM relative to the crystal structure has been demonstrated in small angle x-ray scattering experiments of CaM in solution (Heidorn and Trewhella, 1988), dynamic light scattering (Papish et al., 2002), and pulse-field gradient NMR (Weljie et al., 2003). One of the quantities available from SAXS experiments is the vector length distribution, $P(r)$, which is the frequency distribution of distances between small volume elements within the protein. Fig. 5, *top* and *bottom*, show the radius of gyration and vector length distributions calculated from the simulation, respectively. Decreases in the radius of gyration are correlated with increases in the Cα RMSD (see Fig. 1 *A*): the compaction process is more or less complete at around 5 ns, with only a small change occurring again at 10 ns.

The vector length distribution for the extended crystal structure (Fig. 5, *bottom*) results in two peaks arising from the spatial separation of the two terminal domains. SAXS measurements of the protein in solution also show two peaks but with an increase in the magnitude of the distribution at smaller distances and a noticeable decrease in the maximal length (Trewhella and Krueger, 2002), indicating that CaM is compacted relative to the crystal structure under these conditions. The calculated distribution from the 3-ns mark, with an R_g of 19 Å, is basically identical in both shape and magnitude to the experimental distribution for Ca^{2+}-CaM in solution (Heidorn and Trewhella, 1988). Between 3 and 4 ns, however, the shoulder at long distances disappears, and the distribution becomes unimodal, with an R_g of 17.6 Å. The maximum of this single peak continues to decrease until ~5 ns, at which point the R_g of 15 Å is similar to but somewhat smaller than that of the CaM-smMLCKp complex, shown for comparison.

Following Mehler et al. (1991), the fraction of the total population that exists in a state similar to the extended crystal structure, α, can be estimated from the following equation:

$$\alpha = [\mathrm{Rg2}(\alpha) - \mathrm{Rg2(sim)}]/[\mathrm{Rg2(x\text{-}ray)} - \mathrm{Rg2(sim)}],$$

where $R_g(\alpha)$ is the radius of gyration determined from experiment, $R_g(sim)$ is the value calculated from the simulation, and $R_g(x\text{-}ray)$ is the value calculated from the

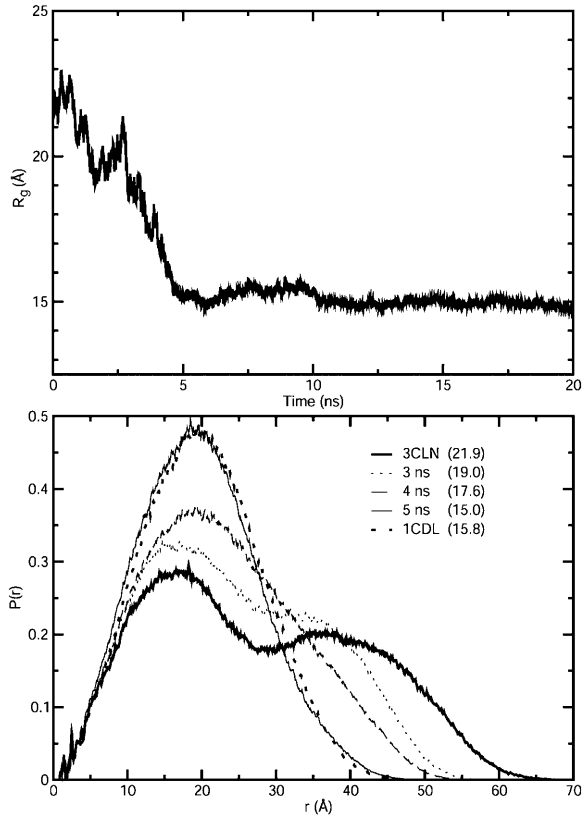

FIGURE 5 (*Top*) Radius of gyration of CaM as a function of simulation time. (*Bottom*) Vector length distribution of CaM in the extended crystal structure (Babu et al., 1988; PDB ID: 3CLN), the CaM-smMLCKp complex (Meador et al., 1992; PDB ID: 1CLN), and at various times during the simulation. Values in brackets give the radius of gyration in angstroms.

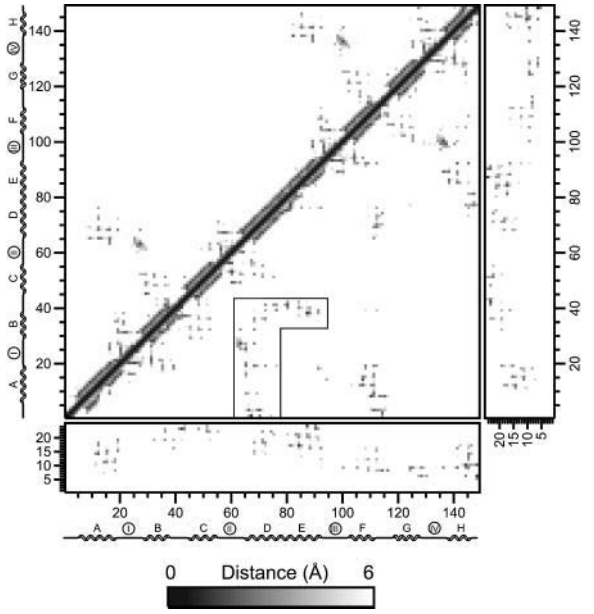

FIGURE 6 Side-chain–side-chain contact maps. The average minimal distance between atoms of each side-chain pair is plotted. All distances ≤5 Å are considered contacts are colored according to the legend. The large matrix shows the contacts between side chains in the extended crystal structure (*upper diagonal*) and as an average over the entire simulation (*lower diagonal*). The two smaller matrices along either axis are identical to each other and show the contacts between CaM and the peptide in the CaM-smMLCKp complex (PDB ID: 1CDL). The secondary structure of CaM is shown along both axes, with the helices and calcium binding sites labeled.

crystal structure. This assumes that the distributions arise from a simple equilibrium between two conformations of CaM, one extended and one compact. It has been noted that the calculated value of α is very sensitive to the values of I_g employed (Sorensen and Shea, 1996). Using a standard analysis program in the GROMACS package, we obtain an average R_g of 14.95 Å from the last 10 ns of the simulation and a value of 21.89 Å for R_g(*x-ray*). Taking the value of 21.5 Å determined for Ca^{2+}-CaM in solution using SAXS (Matsushima et al., 1989) gives a value for α of 94.3%, meaning the compact state in our simulation would represent 6% of the total conformational population. Using a value of 22.8 Å calculated from approximating CaM as three ellipsoids (Heidorn and Trewhella, 1988), the contribution of the compact state rises as high as 16.6%. Taking these values as a possible range, the compact state observed in our simulation would represent a small but significant contribution to the possible conformations of CaM in solution.

To define the regions of calmodulin that interact with each other in the simulation a contact map was calculated. This is shown in Fig. 6, along with maps generated from the crystal structures of Ca^{2+}-CaM and the CaM-smMLCKp complex for comparison. In the crystal structure of Ca^{2+}-CaM (*upper diagonal* of the *square matrix*), there is no interaction between the two terminal domains or between either of these domains and the central linker region. In contrast, the structures from the simulation show a number of close interdomain contacts in specific regions (*lower diagonal* of the *square matrix*). Significantly, the entire length of the central linker (residues 65–92) engages in contacts with the N-terminal lobe, resulting in the cane-shaped pattern (*outlined region*). Side chains in the C-terminal domain around helices F and G also interact with the central linker region and with the first helix of the N-terminal domain. Looking at the contact maps for the CaM-smMLCKp complex, it can be seen that the same regions of CaM responsible for binding to the peptide also form contacts in the compact structure from the simulation: taking any patch of interactions between the terminal lobes in the compact state from the simulation (*larger matrix*), lines drawn to both of the smaller matrices along the bottom and right will connect with peptide-binding patches in the CaM-smMLCKp complex. Despite this, the side chains of hydrophobic cleft residues retain a relatively high degree of solvent accessibility in the compact conformation. Fig. 7 shows the solvent accessible surface areas of methionine side chains in the extended crystal structure, the CaM-smMLCKp complex, and as an average over the last 5 ns of the simulation. With the exception of residues 36 and 76, all the Met side chains have higher solvent accessibilities

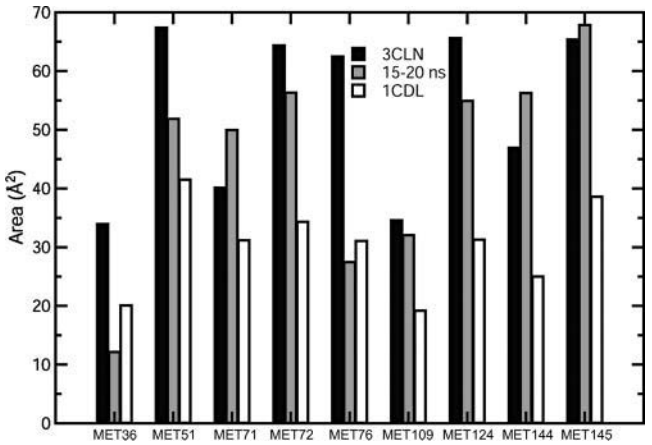

FIGURE 7 Solvent accessibility of methionine side chains in CaM from the extended crystal structure (*solid bars*), as an average between 15 and 20 ns of the simulation (*shaded bars*), and in the CaM-smMLCKp complex (*open bars*). Solvent accessibilities were calculated using the Double Cubic Lattice Method (Eisenhaber et al., 1995).

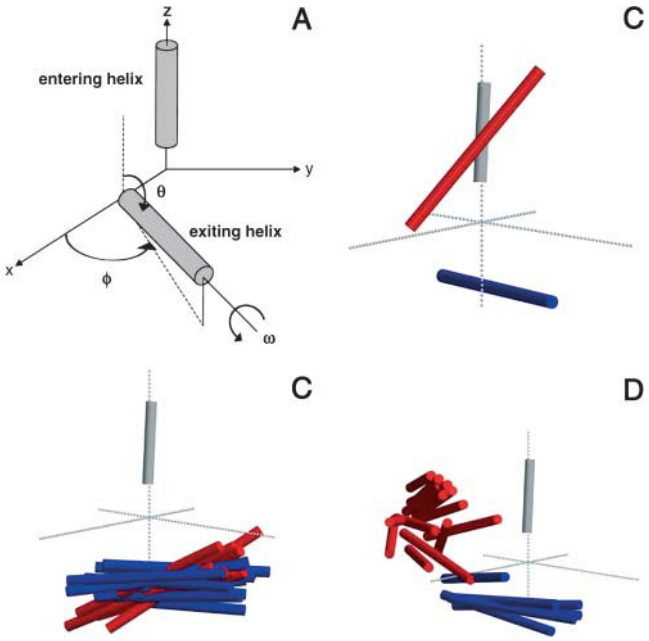

FIGURE 8 VGM analysis. (*A*) Schematic of the vector geometry mapping method. The entering, or first helix, of the EF-hand is superimposed on a reference EF-hand on the $+z$ axis, and the corresponding position of the exiting, or second helix, is evaluated using the angles θ, ϕ, and ω, as shown. Reproduced with permission from Yap et al. (1999). (*B*) Example of an open (*blue*) and a closed (*red*) state from EF-hand II in the Ca^{2+}-CaM (Babu et al., 1988) and apo-CaM (Zhang et al., 1995) structures, respectively. (*C*) Analysis for EF-hand I of CaM, with structures taken every nanosecond of the simulation. (*Blue cylinders*) 0–10 ns and (*red helices*) 10–20 ns. (*D*) Analysis for EF-hand II. (*Blue cylinders*) 0–5 ns and (*red cylinders*) 6–20 ns.

than in the CaM-smMLCKp complex and are comparable or even greater than in the Ca^{2+}-CaM crystal structure. The same trend was observed for other hydrophobic cleft residues (data not shown).

EF-hand conformational changes

We have employed vector geometry mapping (Yap et al., 1999, 2002) to monitor the behavior of the EF-hand domains in our simulation. Corresponding to its higher rigidity, all EF-hands in the C-terminal lobe maintain an open conformation throughout the simulation. However, conformational changes were observed in the EF-hands of the N-terminal lobe. Fig. 8 *A* shows a schematic of a VGM axis system and the angles used to define orientations between the two helices of an EF-hand domain. For reference, Fig. 8 *B* shows the open (*blue*) and closed (*red*) conformations of EF-hand II from the structures of Ca^{2+}-CaM (Babu et al., 1988) and apo-CaM (Zhang et al., 1995), respectively. Fig. 8, *C* and *D*, shows the analysis for EF-hands I and II of the N-terminal domain, respectively, using structures taken each nanosecond of the simulation. In the case of the EF-hand I, there is a small but noticeable difference between the interhelical angles before and after 10 ns. The increase in the value of θ, however, is much less than expected for a typical transition from the open to closed state. In the case of EF-hand II, the change from an open to a closed state proceeds gradually up until around 5 ns. A large transition takes place in the next nanosecond and is essentially complete after this time, with relatively minor changes in orientation of the helices between 6 and 10 ns.

Interdomain coupling

Interactions between specific residues in the central linker region and the N-terminal domain have been implicated in reducing the calcium affinity of EF-hands I and II in PCaM (Faga et al., 2003). Since the EF-hands of CaM assume a closed conformation in the absence of calcium, correlation between interresidue contacts and the closing of EF-hand II in the simulation may describe a mechanism by which this phenomenon occurs. Fig. 9 shows contact maps calculated every 2 ns for the side chains of residues 74–80 and the rest of CaM. Several interactions develop between these residues and the N-terminal lobe in the first 2 ns of the simulation. These are primarily limited to the basic residues Arg-74 and Lys-77 in the central linker and polar residues near the N-terminus (Asp-2, Gln-3, and Gln-8), although Lys-75 also interacts with Ile-52 and Val-55 in what is presumably a hydrophobic interaction (Padmanabhan et al., 1996). The strength of the interactions involving the N-terminal residues increases between 2 and 4 ns, with an average decrease in the interside-chain distance of about an angstrom in all cases. As in the first 2 ns, Lys-77 forms the largest number of interactions with the N-terminus, whereas residues Glu-78, Gln-79, and Asp-80 form little to no contacts. All the interactions decrease between 4 and 6 ns and then disappear entirely between 6 and 8 ns.

Starting in the time frame between 4 and 6 ns, the side chains of residues 74–80 also make contact with those near

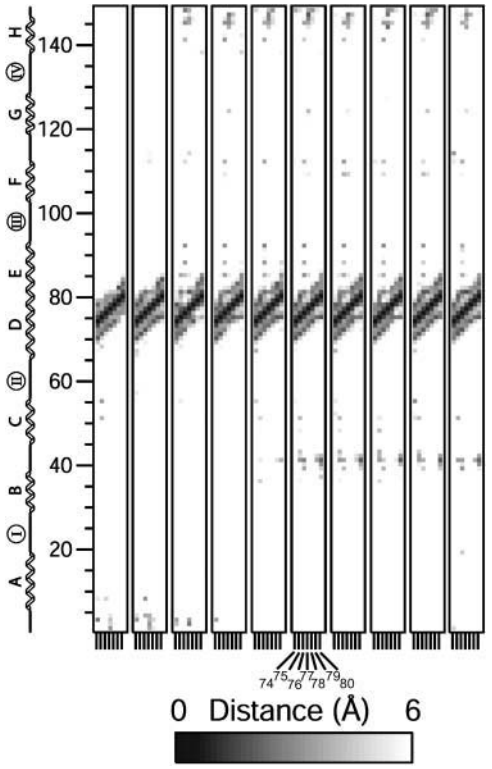

FIGURE 9 Side-chain–side-chain contacts between residues 74–80 and the rest of CaM as a function of simulation time. Contacts were calculated as in Fig. 6 and averaged over 2-ns windows of the simulation. Contact maps for successive windows proceed from left to right in the figure. The secondary structure of CaM is shown along the *y* axis, with the helices and calcium binding sites labeled.

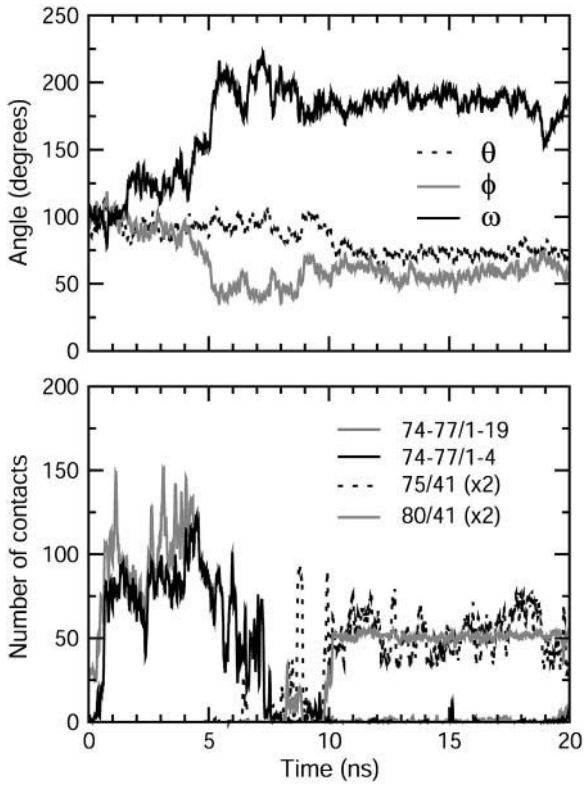

FIGURE 10 Correlation of side-chain–side-chain contacts and the closing of EF-hand II. (*Top*) Interhelical angles from the VGM analysis (see Fig. 8). (*Bottom*) Number of contacts between specific sets of residues (see legend) as a function of simulation time. Distances between all atoms of the relevant side chains were calculated, and any distance ≤5 Å was considered a contact. The number of contacts was multiplied by a factor of two in some cases for ease of presentation (see *legend*).

the C-terminus and in the regions connecting individual EF-hand domains in both terminal lobes. Among these, contacts between Gln-41 in the N-terminal lobe and residues Lys-75 and Asp-80 of the central linker are particularly strong. There is experimental evidence for these interactions: the contact between Lys-75 and Gln-41 can be seen in an NMR structure of apo-CaM (Sorensen et al., 2002). Also, a 10-fold decrease in the proteolytic (thrombin) susceptibility of the Arg-37–Ser-38 peptide bond in $CaM_{1–80}$ compared to $CaM_{1–75}$ from rat (Sorensen and Shea, 1998) provides indirect evidence for interactions like the one observed between Gln-41 and Asp-80. Interactions near the C-terminus are dominated by hydrophobic interactions between linker residues Met-76 and Lys-77 and C-terminal residues Phe-141, Met-144, and Met-145.

Fig. 10 shows the correlation between various interresidue contacts and the interhelical angles of EF-hand II during the simulation. The onset of interactions between residues 74–77 and those near the N-terminus correlates with large changes in ω. Changes in this interhelical angle were shown to be particularly diagnostic of opening or closing of an EF-hand (Yap et al., 1999). Interaction of residues 74–77 with helix A are dominated by the first four residues of CaM, as can be seen by comparing the number of interactions involving these residues with the numbers for the entire first helix (residues 1–19). Shortly after these interactions reach their maximum at 5 ns, changes in the interhelical angles reach relatively stable values, marking the end of the transition of the EF-hand from open to closed. Interactions between Lys-74 and Asp-80 are among the strongest interactions between the central linker and the entire N-terminal lobe in the latter stages of the simulation and are shown as an example of the contacts between the central linker and the region between helices B and C. Although these contacts do not arise until after the closing of the EF-hand, they may play a role in stabilizing the closed conformation. The interaction between Gln-41 and Asp-80 is particularly stable in the last 10 ns of the simulation.

DISCUSSION

Various features of the simulation are in agreement with experimental results. The breakdown in helical structure between residues 75–81 is in accordance with ^{15}N order parameters (Barbato et al., 1992) and earlier simulations of both CaM (Wriggers et al., 1998; Yang et al., 2001) and the

central linker helix (Van der Spoel et al., 1996). Although experimental order parameters for residues 82–86 are higher than for 75–81, the proximity of acidic residues Asp-80, Glu-82, Glu-83, Glu-84, Glu-87, Asp-93, and Asp-95 may cause electrostatic repulsions between side chains in this region, resulting in higher conformational disorder in the central helix at low ionic strength (Sun et al., 1999). More than one example of acidic residue pairs spaced three (Asp-80–Glu-83 and Glu-84–Glu-87) and four (Asp-80–Glu-84 and Glu-83–Glu-87) residues apart in this region can be found. Due to their proximity on the same face of an α-helix, charged residues with these spacings can significantly affect helical stability (Marqusee and Baldwin, 1987). As our simulation included only those counterions necessary to render the system electrostatically neutral, the electrostatic interactions between the acidic residues in this region will be stronger than in a solution that more closely models physiological ionic strength. However, a distortion of this helical turn was also observed in an earlier 4-ns simulation of Ca^{2+}-CaM that included 40 sodium and 24 chloride counterions, respectively (Yang et al., 2001). That the loss of a salt bridge between Glu-82 and Lys-86 in this helical turn contributes so significantly to the disruption of the central linker and subsequent compaction of the protein demonstrates the strong effect this highly charged region can exert on the relative separation of the individual CaM domains.

A survey of distances between favorably interacting side-chain–side-chain pairs over the course of the simulation revealed that the hydrogen bond between Glu-82 and Tyr-138 was among the first interactions lost, which helps to initiate the compaction process. The importance of this interaction in maintaining the elongated structure of CaM has been demonstrated experimentally: the substitution of Tyr-138 with either a Phe or Gln residue significantly reduces the average spatial separation between the terminal lobes and increases the conformational heterogeneity of the central linker (Sun et al., 2001).

Our simulation indicates that the terminal domains of CaM can interact directly in solution. A relatively early study of CaM, in which the N- and C-terminal domains were chemically cross-linked in solution, suggested that the distance between residues 3 and 146 can be no more than 19 Å apart, compared to the 37-Å distance observed in the crystal structure (Persechini and Kretsinger, 1988). Since that time, interactions between the domains of CaM have been inferred from proteolytic footprinting (Pedigo and Shea, 1995; Shea et al., 1996, 2000) and optical spectroscopy studies (Yazawa et al., 1990), as well as comparisons between the properties of whole CaM and its N- and C-terminal domain fragments (Lee and Klevit, 2000; Masino et al., 2000; Sellers et al., 1991; Sorensen and Shea, 1998). Relatively small perturbations such as single residue substitutions (Sun et al., 2001) and the deletion of the four C-terminal residues in CaM (145–148; Yin et al., 2000) can lead to smaller separations and between the terminal domains and structural collapse of the protein, respectively. The binding of small molecules such as trifluoperazine and W-7 can also induce globular structure in Ca^{2+}-CaM (Cook et al., 1994; Osawa et al., 1999; Vandonselaar et al., 1994). Perhaps the most convincing evidence supporting the possibility of interdomain interactions in Ca^{2+}-CaM comes from a recently published high resolution (1.7 Å) crystal structure, in which the protein adopts a globular compact shape (Fallon and Quiocho, 2003). The R_g of this conformation is 14.8 Å, which is very close to the average value calculated from the last 10 ns of the simulation (14.95 Å). Interactions between the two terminal domains in the compact crystal structure are substantial, with 16 hydrogen bonds and 24 van der Waals contacts being formed (Fallon and Quiocho, 2003). Owing to the fact that the terminal domains remain in a *trans* orientation with respect to each other in the compact crystal structure, there are significant differences between the residues involved in interdomain contacts and those observed in our simulation. However, there are also some intriguing similarities, particularly contacts between the EF-hand loops in each domain (Gln-41 and Gln-114 in the crystal structure). On the whole, contacts between domains in both the crystal structure and the simulation involve residues within the promiscuous, hydrophobic patches of each domain. It should be noted, however, that the compact structure observed in our simulation is most likely due to the extremely low ionic strength conditions. In an earlier 4-ns simulation of CaM, a sufficient number of counterions were added to model an ionic strength of 0.15 M (Yang et al., 2001). In this simulation, the protein remained within a 2–3-Å RMSD of the crystal structure. In comparison to our results, relatively minor structural distortions of the central helix were observed. Furthermore, fluorescence resonance energy transfer (FRET) experiments employing a label on the C-terminal domain and an acceptor on the N-terminal domain show a narrow Gaussian distribution of distances for the central linker centered around 31 Å at physiological ionic strength (Sun et al., 1999). This would indicate that compact structures like the ones in our simulation make a small contribution to the accessible conformations under these conditions. In the same study, an increase in the conformational heterogeneity of the central linker was observed at low ionic strength (Sun et al., 1999), which likely explains the large conformational changes observed in our simulation.

A curious aspect of our results is the discrepancy of timescales with respect to experiment: we observe the structural collapse of calmodulin in <10 ns, whereas rearrangements of the terminal domains with respect to each other are slower than 9–12 ns (Qin and Squier, 2001). Once again, this could be due to the fact that we have carried out our simulation at extremely low ionic strength, with the relatively rapid structural collapse being due to the much lower stability of the central helix.

Despite the similarity between the interdomain interface in the simulation and the CaM-smMLCKp interface (Meador et al., 1992), the solvent accessibility of Met residues in the compact state leads us to suggest that this conformation would still be capable of binding to a target protein. This is consistent with the observation that the deletion of residues 145–148 of *Paramecium* CaM led to the collapse of the structure, but did not prevent its activation of plasma membrane Ca-ATPase (Yin et al., 2000).

Although the compact state of calmodulin from the simulation appears stable for ~10 ns, it is entirely possible that the protein would once again assume an extended conformation in a longer simulation. The relatively small estimated contribution of the compact state to distributions of CaM in solution (~6–16%) would indicate that conformations of this type are short lived and are probably inaccessible to most experimental techniques. For this reason, we do not feel that the absence of observable interdomain contacts in structural studies of vertebrate Ca^{2+}-CaM to date precludes the transient existence of such conformations in solution. Also, the character of the interface between the domains in the compact state is reasonable in that the interactions are mediated by the same regions of CaM responsible for interacting with the CaM-binding regions of target proteins. SAXS measurements on CaM from *Saccharomyces cerevisiae* indicate a globular shape upon binding calcium (Yoshino et al., 1996). This was recently confirmed in a structural NMR study (Lee and Klevit, 2000), which further show that the two terminal domains interact through their hydrophobic surfaces.

One of the more interesting aspects of our simulation is the apparent correlation of conformational changes in the second EF-hand with contacts formed between the central linker residues 74–77 and the N-terminus. The agreement between the specific residue pairs making contact in the simulation and the chemical shift changes between the $PCaM_{1-74}$ and $PCaM_{1-80}$ constructs (Faga et al., 2003) is very good, and the correlation between these contacts and the closing of EF-hand II describes a mechanism by which they affect calcium affinity in the N-domain. Although not studied by NMR, the thermostability and calcium affinity of the CaM_{1-75} and CaM_{1-80} constructs from rat have also been compared and reveal similar trends to the same constructs from *Paramecium* (Sorensen et al., 2002). Owing to the high sequence homology of residues 76–80 in CaM from many species (Faga et al., 2003), our simulation results could have broad applicability.

Despite the localization of these contacts to the helix A of CaM, the first EF-hand does not undergo a significant conformational change from open to closed. The examination of structures from the start and end of the simulation shows that the unwinding of the N-terminal region and its contacts with residues in the central linker may actually prevent a reorientation of the helices in EF-hand I (data not shown). The effect on EF-hand II may be an indication of propagated effects throughout the entire N-terminal domain, as suggested from experimental results (Faga et al., 2003).

In addition to a strong interaction between Lys-75 and Gln-41 that has been suggested experimentally (Ababou and Desjarlais, 2001), we also see close contacts between Gln-41 and Asp-80, even though residues beyond Lys-77 were not observed to have any effect on calcium binding affinity (Faga et al., 2003). Our results indicate that this residue may contribute to interdomain coupling in whole CaM. Interactions between the terminal lobes may also be important: most of the interactions between the second EF-hand and the C-terminal domain are due to residues near the region connecting EF-hands III and IV (see Fig. 6) and indicate that the cooperativity between calcium binding in the terminal lobes may, in some instances, result from direct contacts between the EF-hand domains. However, it is important to note that interdomain coupling need not progress via a mechanism involving contacts between the terminal domains: by monitoring chemical shift and intensity changes in a calcium titration of CaM via NMR, it has been suggested that conformational changes within the linker region in response to calcium binding may provide the means by which the terminal domains communicate (Jaren et al., 2002). At this time, the precise mechanism of interdomain coupling in CaM is incompletely understood. It should be noted that the N-domain of CaM (nCaM) construct simulated earlier consists of residues 1–77 (Vigil et al., 2001) and therefore contains all the C-terminal residues important in lowering the calcium affinity in the N-domain (Faga et al., 2003). A reanalysis of this simulation focusing on the correlation of interresidue contacts and closing of the EF-hand domains would be useful in further testing the differences between an isolated N-terminal domain and whole CaM.

This work was supported by an operating grant from the Alberta Heart and Stroke Foundation and the Alberta Synchrotron Institute. H.J.V. holds a Scientist Award from the Alberta Heritage Foundation for Medical Research. C.M.S was the recipient of a Doctoral Research Award from the Canadian Institutes of Health Research.

REFERENCES

Ababou, A., and J. R. Desjarlais. 2001. Solvation energetics and conformational change in EF-hand proteins. *Protein Sci.* 10:301–312.

Aliste, M., J. L. MacCallum, and D. P. Tieleman. 2003. Molecular dynamics simulations of pentapeptides at interfaces: salt bridge and cation-π interactions. *Biochemistry.* 42:8976–8987.

Babu, Y. S., C. E. Bugg, and W. J. Cook. 1988. Structure of calmodulin refined at 2.2 Å resolution. *J. Mol. Biol.* 204:191–204.

Barbato, G., M. Ikura, L. E. Kay, R. W. Pastor, and A. Bax. 1992. Backbone dynamics of calmodulin studied by ^{15}N relaxation using inverse detected two-dimensional NMR spectroscopy: the central helix is flexible. *Biochemistry.* 31:5269–5278.

Barton, N. P., C. S. Verma, and L. S. A. Caves. 2002. Inherent flexibility of calmodulin domains: a normal-mode analysis study. *J. Phys. Chem. B.* 106:11036–11040.

Berendsen, H. J. C., J. P. M. Postma, A. DiNola, and J. R. Haak. 1984. Molecular dynamics with coupling to an external bath. *J. Chem. Phys.* 81:3684–3690.

Berendsen, H. J. C., J. P. M. Postma, W. F. van Gunsteren, and J. Hermans. 1981. Interaction models for water in relation to protein hydration. *In* Intermolecular Forces. B. Pullman, editor. D. Reidel Publishing Company, Dordrecht, The Netherlands. 331–42.

Chattopadhyaya, R., W. E. Meador, A. R. Means, and F. A. Quiocho. 1992. Calmodulin structure refined at 1.7 Å resolution. *J. Mol. Biol.* 228:1177–1192.

Chou, J. J., S. Li, C. B. Klee, and A. Bax. 2001. Solution structure of Ca(2+)-calmodulin reveals flexible hand-like properties of its domains. *Nat. Struct. Biol.* 8:990–997.

Cook, W. J., L. J. Walter, and M. R. Walter. 1994. Drug binding by calmodulin: crystal structure of a calmodulin-trifluoperazine complex. *Biochemistry.* 33:15259–15265.

Eisenhaber, F., P. Lijnzaad, P. Argos, C. Sander, and M. Scharf. 1995. The double cubic lattice method: efficient approaches to numerical-integration of surface-area and volume and to dot surface contouring of molecular assemblies. *J. Comput. Chem.* 16:273–284.

Faga, L. A., B. R. Sorensen, W. S. VanScyoc, and M. A. Shea. 2003. Basic interdomain boundary residues in calmodulin decrease calcium affinity of sites I and II by stabilizing helix-helix interactions. *Proteins.* 50: 381–391.

Fallon, J. L., and F. A. Quiocho. 2003. A closed compact structure of native Ca(2+)-calmodulin. *Structure (Camb.).* 11:1303–1307.

Feenstra, K. A., B. Hess, and H. J. C. Berendsen. 1999. Improving efficiency of large time-scale molecular dynamics simulations of hydrogen-rich systems. *J. Comput. Chem.* 20:786–798.

Heidorn, D. B., and J. Trewhella. 1988. Comparison of the crystal and solution structures of calmodulin and troponin C. *Biochemistry.* 27: 909–915.

Hoeflich, K. P., and M. Ikura. 2002. Calmodulin in action: diversity in target recognition and activation mechanisms. *Cell.* 108:739–742.

Humphrey, W., A. Dalke, and K. Schulten. 1996. VMD: visual molecular dynamics. *J. Mol. Graph.* 14:33–38.

Ikura, M., G. M. Clore, A. M. Gronenborn, G. Zhu, C. B. Klee, and A. Bax. 1992. Solution structure of a calmodulin-target peptide complex by multidimensional NMR. *Science.* 256:632–638.

Ishida, H. and H. J. Vogel. 2004. Protein-peptide interaction studies demonstrate versatility of calmodulin target protein binding. *Prot. Pept. Lett.* In press.

Jaren, O. R., J. K. Kranz, B. R. Sorensen, A. J. Wand, and M. A. Shea. 2002. Calcium-induced conformational switching of Paramecium calmodulin provides evidence for domain coupling. *Biochemistry.* 41: 14158–14166.

Jorgensen, W. L., J. Chandrasekhar, J. D. Madura, R. W. Impey, and M. L. Klein. 1983. Comparison of simple potential functions for simulating liquid water. *J. Chem. Phys.* 79:926–935.

Kabsch, W., and C. Sander. 1983. Dictionary of protein secondary structure: pattern recognition of hydrogen-bonded and geometrical features. *Biopolymers.* 22:2577–2637.

Komeiji, Y., Y. Ueno, and M. Uebayasi. 2002. Molecular dynamics simulations revealed Ca(2+)-dependent conformational change of Calmodulin. *FEBS Lett.* 521:133–139.

Lee, S. Y., and R. E. Klevit. 2000. The whole is not the simple sum of its parts in calmodulin from S. cerevisiae. *Biochemistry.* 39:4225–4230.

Lindahl, E., B. Hess, and D. van der Spoel. 2001. GROMACS 3.0: a package for molecular simulation and trajectory analysis. *J. Mol. Model.* 7:306–317.

Liu, H. Y., F. Müller-Plathe, and W. F. van Gunsteren. 1995. A force field for liquid dimethyl sulfoxide and physical properties of liquid dimethyl sulfoxide calculated using molecular dynamics simulation. *J. Am. Chem. Soc.* 117:4363–4366.

Mark, A. E., S. P. van Helden, P. E. Smith, L. H. M. Janssen, and W. F. van Gunsteren. 1994. Convergence properties of free energy calculations: alpha cyclodextrin complexes as a case study. *J. Am. Chem. Soc.* 116: 6293–6302.

Marqusee, S., and R. L. Baldwin. 1987. Helix stabilization by Glu-. . .Lys+ salt bridges in short peptides of de novo design. *Proc. Natl. Acad. Sci. USA.* 84:8898–8902.

Masino, L., S. R. Martin, and P. M. Bayley. 2000. Ligand binding and thermodynamic stability of a multidomain protein, calmodulin. *Protein Sci.* 9:1519–1529.

Matsushima, N., Y. Izumi, T. Matsuo, H. Yoshino, T. Ueki, and Y. Miyake. 1989. Binding of both Ca^{2+} and mastoparan to calmodulin induces a large change in the tertiary structure. *J. Biochem. (Tokyo).* 105:883–887.

Meador, W. E., A. R. Means, and F. A. Quiocho. 1992. Target enzyme recognition by calmodulin: 2.4 Å structure of a calmodulin-peptide complex. *Science.* 257:1251–1255.

Mehler, E. L., J. L. Pascual-Ahuir, and H. Weinstein. 1991. Structural dynamics of calmodulin and troponin C. *Protein Eng.* 4:625–637.

Osawa, M., S. Kuwamoto, Y. Izumi, K. L. Yap, M. Ikura, T. Shibanuma, H. Yokokura, H. Hidaka, and N. Matsushima. 1999. Evidence for calmodulin inter-domain compaction in solution induced by W-7 binding. *FEBS Lett.* 442:173–177.

Padmanabhan, S., E. J. York, J. M. Stewart, and R. L. Baldwin. 1996. Helix propensities of basic amino acids increase with the length of the side-chain. *J. Mol. Biol.* 257:726–734.

Papish, A. L., L. W. Tari, and H. J. Vogel. 2002. Dynamic light scattering study of calmodulin-target peptide complexes. *Biophys. J.* 83:1455–1464.

Pedigo, S., and M. A. Shea. 1995. Quantitative endoproteinase GluC footprinting of cooperative Ca^{2+} binding to calmodulin: proteolytic susceptibility of E31 and E87 indicates interdomain interactions. *Biochemistry.* 34:1179–1196.

Persechini, A., and R. H. Kretsinger. 1988. The central helix of calmodulin functions as a flexible tether. *J. Biol. Chem.* 263:12175–12178.

Qin, Z., and T. C. Squier. 2001. Calcium-dependent stabilization of the central sequence between Met(76) and Ser(81) in vertebrate calmodulin. *Biophys. J.* 81:2908–2918.

Sellers, P., J. Laynez, E. Thulin, and S. Forsen. 1991. Thermodynamics of Ca^{2+} binding to calmodulin and its tryptic fragments. *Biophys. Chem.* 39:199–204.

Shea, M. A., B. R. Sorensen, S. Pedigo, and A. S. Verhoeven. 2000. Proteolytic footprinting titrations for estimating ligand-binding constants and detecting pathways of conformational switching of calmodulin. *Methods Enzymol.* 323:254–301.

Shea, M. A., A. S. Verhoeven, and S. Pedigo. 1996. Calcium-induced interactions of calmodulin domains revealed by quantitative thrombin footprinting of Arg37 and Arg106. *Biochemistry.* 35:2943–2957.

Sorensen, B. R., L. A. Faga, R. Hultman, and M. A. Shea. 2002. An interdomain linker increases the thermostability and decreases the calcium affinity of the calmodulin N-domain. *Biochemistry.* 41: 15–20.

Sorensen, B. R., and M. A. Shea. 1996. Calcium binding decreases the stokes radius of calmodulin and mutants R74A, R90A, and R90G. *Biophys. J.* 71:3407–3420.

Sorensen, B. R., and M. A. Shea. 1998. Interactions between domains of apo calmodulin alter calcium binding and stability. *Biochemistry.* 37:4244–4253.

Spera, S., M. Ikura, and A. Bax. 1991. Measurement of the exchange rates of rapidly exchanging amide protons: application to the study of calmodulin and its complex with a myosin light chain kinase fragment. *J. Biomol. NMR.* 1:155–165.

Sun, H., D. Yin, L. A. Coffeen, M. A. Shea, and T. C. Squier. 2001. Mutation of Tyr138 disrupts the structural coupling between the opposing domains in vertebrate calmodulin. *Biochemistry.* 40:9605–9617.

Sun, H., D. Yin, and T. C. Squier. 1999. Calcium-dependent structural coupling between opposing globular domains of calmodulin involves the central helix. *Biochemistry.* 38:12266–12279.

Trewhella, J., and J. K. Krueger. 2002. Small-angle solution scattering reveals information on conformational dynamics in calcium-binding proteins and in their interactions with regulatory targets. *Methods Mol. Biol.* 173:137–159.

Van Buuren, A. R., S. J. Marrink, and H. J. C. Berendsen. 1993. A molecular dynamics study of the decane water interface. *J. Phys. Chem.* 97:9206–9212.

Van der Spoel, D., B. L. de Groot, S. Hayward, H. J. Berendsen, and H. J. Vogel. 1996. Bending of the calmodulin central helix: a theoretical study. *Protein Sci.* 5:2044–2053.

Van Gunsteren, W. F., and H. J. C. Berendsen. 1987. Gromos-87 Manual. Biomos B.V., Groningen, The Netherlands.

Vandonselaar, M., R. A. Hickie, J. W. Quail, and L. T. Delbaere. 1994. Trifluoperazine-induced conformational change in Ca(2+)-calmodulin. *Nat. Struct. Biol.* 1:795–801.

Vigil, D., S. C. Gallagher, J. Trewhella, and A. E. Garcia. 2001. Functional dynamics of the hydrophobic cleft in the N-domain of calmodulin. *Biophys. J.* 80:2082–2092.

Vorherr, T., O. Kessler, A. Mark, and E. Carafoli. 1992. Construction and molecular dynamics simulation of calmodulin in the extended and in a bent conformation. *Eur. J. Biochem.* 204:931–937.

Weinstein, H., and E. L. Mehler. 1994. Ca(2+)-binding and structural dynamics in the functions of calmodulin. *Annu. Rev. Physiol.* 56: 213–236.

Weljie, A. M., A. P. Yamniuk, H. Yoshino, Y. Izumi, and H. J. Vogel. 2003. Protein conformational changes studied by diffusion NMR spectroscopy: application to helix-loop-helix calcium binding proteins. *Protein Sci.* 12:228–236.

Wilson, M. A., and A. T. Brunger. 2000. The 1.0 Å crystal structure of Ca(2+)-bound calmodulin: an analysis of disorder and implications for functionally relevant plasticity. *J. Mol. Biol.* 301:1237–1256.

Wriggers, W., E. Mehler, F. Pitici, H. Weinstein, and K. Schulten. 1998. Structure and dynamics of calmodulin in solution. *Biophys. J.* 74:1622–1639.

Yamniuk, A. P., and H. J. Vogel. 2004. Calmodulin's flexibility allows for promiscuity in its interactions with target proteins and peptides. *Mol. Biotechnol.* 27:33–57.

Yang, C., G. S. Jas, and K. Kuczera. 2001. Structure and dynamics of calcium-activated calmodulin in solution. *J. Biomol. Struct. Dyn.* 19: 247–271.

Yang, C., and K. Kuczera. 2002. Molecular dynamics simulations of calcium-free calmodulin in solution. *J. Biomol. Struct. Dyn.* 19:801–819.

Yap, K. L., J. B. Ames, M. B. Swindells, and M. Ikura. 1999. Diversity of conformational states and changes within the EF-hand protein superfamily. *Proteins.* 37:499–507.

Yap, K. L., J. B. Ames, M. B. Swindells, and M. Ikura. 2002. Vector geometry mapping. A method to characterize the conformation of helix-loop-helix calcium-binding proteins. *Methods Mol. Biol.* 173:317–324.

Yap, K. L., T. Yuan, T. K. Mal, H. J. Vogel, and M. Ikura. 2003. Structural basis for simultaneous binding of two carboxy-terminal peptides of plant glutamate decarboxylase to calmodulin. *J. Mol. Biol.* 328:193–204.

Yazawa, M., F. Matsuzawa, and K. Yagi. 1990. Inter-domain interaction and the structural flexibility of calmodulin in the connecting region of the terminal two domains. *J. Biochem. (Tokyo).* 107:287–291.

Yin, D., H. Sun, D. A. Ferrington, and T. C. Squier. 2000. Closer proximity between opposing domains of vertebrate calmodulin following deletion of Met(145)-Lys(148). *Biochemistry.* 39:10255–10268.

Yoshino, H., Y. Izumi, K. Sakai, H. Takezawa, I. Matsuura, H. Maekawa, and M. Yazawa. 1996. Solution X-ray scattering data show structural differences between yeast and vertebrate calmodulin: implications for structure function. *Biochemistry.* 35:2388–2393.

Yuan, T., H. Ouyang, and H. J. Vogel. 1999a. Surface exposure of the methionine side chains of calmodulin in solution. A nitroxide spin label and two-dimensional NMR study. *J. Biol. Chem.* 274:8411–8420.

Yuan, T., M. P. Walsh, C. Sutherland, H. Fabian, and H. J. Vogel. 1999b. Calcium-dependent and -independent interactions of the calmodulin-binding domain of cyclic nucleotide phosphodiesterase with calmodulin. *Biochemistry.* 38:1446–1455.

Zhang, M., T. Tanaka, and M. Ikura. 1995. Calcium-induced conformational transition revealed by the solution structure of apo calmodulin. *Nat. Struct. Biol.* 2:758–767.